Chapter 15
Smart Platforms for Biomedical Applications

Tarun Vemulkar and Russell P. Cowburn

Abstract This chapter provides an overview of the various types of magnetic micro- and nanoparticle systems used in biomedical applications. We broadly divide particle types into colloidally synthesized and lithographically defined on silicon wafers. The applications relevant to each particle type are highlighted followed by research case studies. Each case study highlights a novel approach to the engineering of magnetic particles for a specific application. Finally, future perspectives for the field are described with an emphasis on the challenges remaining to be solved for all the main application areas of magnetic particles.

15.1 Colloidally Synthesized Nanoparticles

Superparamagnetic iron oxide nanoparticles (SPIONs) have largely been the foundational materials system for the biomedical applications of magnetic nanoparticles [1–8]. These γ-Fe_2O_3 (maghemite)- or Fe_3O_4 (magnetite)-based single domain nanoparticles possess a net zero remanent magnetic state due to the thermal fluctuation of their magnetic moments via Néel–Brown relaxation [9, 10]. SPIONs have been particularly useful in the biomedical space because of their biocompatibility, relative ease of colloidal chemistry-based fabrication, and resistance to magnetically driven aggregation in the absence of an applied field. Colloidally fabricated nanoparticles may also be synthesized at sizes larger than the superparamagnetic limit at which point they become single domain nanoparticles, and then multidomain. Other materials including Ni- and Co-based nanoparticles [11, 12], as well as mixed oxides [11–16] based on Fe and other transition metals are also of relevance to this space.

T. Vemulkar (✉) · R. P. Cowburn
Cavendish Laboratory, University of Cambridge, JJ Thomson Ave, Cambridge CB3 0HE, UK
e-mail: tv243@cam.ac.uk

D. Peddis et al. (eds.), *New Trends in Nanoparticle Magnetism*,
Springer Series in Materials Science 308,
https://doi.org/10.1007/978-3-030-60473-8_15

The most clinically advanced application involves the use of magnetic nanoparticles as contrast agents in the imaging of biological tissue [17–22]. This encompasses the more established technique of magnetic resonance imaging (MRI) and the comparatively more recent approach of magnetic particle imaging (MPI) [23].

For therapeutics, the heat generated when magnetic nanoparticles are exposed to alternating magnetic fields in the 100–1000 kHz range has been harnessed as a cell killing mechanism [24–29]. By increasing the temperature of the environment near a concentrated dose of SPIONS in biological tissue such as a tumour for example, a localized, triggered, tumour destroying therapeutic may be realized. This heat generation may also be used as the trigger for a thermally sensitive drug delivery mechanism [24–29].

Magnetic nanoparticles are also used extensively within the biomedical research space due to the ease of mechanical actuation of magnetic materials. This allows for their deployment in assays where biomolecules may need to be captured, concentrated, and re-suspended in solution [30, 31]. With the development of extremely sensitive magnetic field sensors based on magnetoresistance device architectures [32–34], magnetic nanoparticles may also be used as the detection moiety in biosensing systems instead of simply as a means of purifying samples for the elution of analytes. And finally, mechanical actuation has also been used to stimulate cells and tissue to trigger downstream phenotypic effects [35], as well as trigger cell death [36] in a different take on the therapeutic approach.

15.1.1 Applications

15.1.1.1 Magnetic Resonance Imaging

Magnetic resonance imaging (MRI) is a ubiquitous tool that has given clinicians the ability to achieve huge improvements in soft tissue contrast, opening a wide array of diagnostic procedures beyond that offered by X-ray radiation. Rooted firmly in the principles of nuclear magnetic resonance [37, 38], MRI imaging is based on the relaxation of the nuclear magnetic spins of hydrogen atoms, present in water and organic material that comprises human tissue (Fig. 15.1).

Since the inherent variation in signal between tissues is often insufficient for clinical requirements, contrast agents are used to significantly enhance MRI signals by modifying the values of the characteristic relaxation times, T_1, T_2, and T_2* [39–41], of the nuclear spins in the applied static and dynamic fields of an MRI scanner. T_1 contrast agents work by significantly shortening the T_1 of hydrogen nuclei in their vicinity, thereby significantly boosting the T_1 positive signal. High-spin paramagnetic ions are typical T_1 contrast agents [42–45], of which Gd^{3+} [42, 46, 47] is the clinical contrast agent of choice when chelated with various organic molecules for safety. However, significant effort is being expended in to the incorporation of Gd^{3+} into nanoparticles [48–51] to increase sensitivity, specificity, and reduce clearance time and toxicity (particularly nephrotic cystic fibrosis in patients with impaired

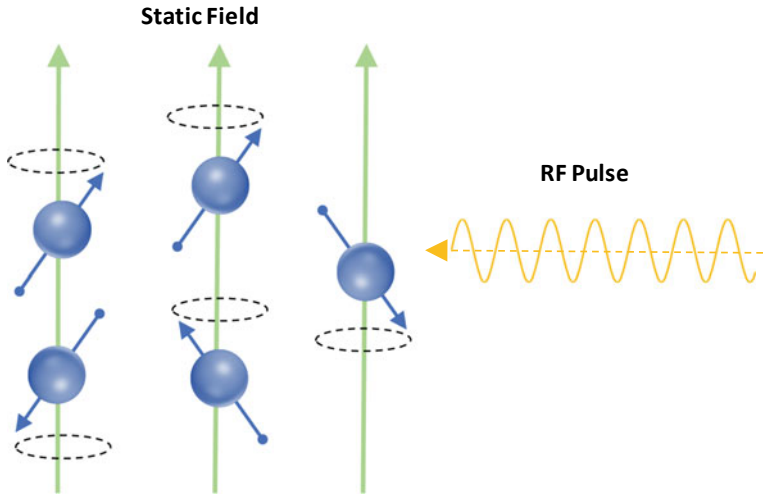

Fig. 15.1 In an MRI measurement, hydrogen nuclei in the water and hydrocarbons in tissue align in and precess to a static field of 1.5–3 T. An orthogonal RF pulse at the Larmor precession frequency of the nuclei misaligns them to the static field and causes them to precess in phase with each other. Over time, they relax back to alignment with the static field with a characteristic time T_1 and dephase with each other with a characteristic time T_2. T_2* is the observed T_2 and is usually much shorter due to field inhomogeneities

renal function [52]). Further optimization along this direction may prove extremely beneficial to the space of MRI contrast agents.

SPIONS, on the other hand, are used as T_2* contrast agents [48–51, 53] and operate by shortening T_2* relaxation times and thus locally reducing image intensity (termed negative contrast agents). The local magnetic field gradient and inhomogeneity from the presence of the magnetic nanoparticles results in rapid dephasing of the nuclear moments causing a significant reduction in signal. It should be noted that magnetic nanoparticles influence T_2* relaxation times in a much larger volume than T_1 contrast agents because of the relatively strong stray fields from their high magnetic moment [20, 54]. Particularly relevant here are SPIONs of sizes of a few hundred nanometres, as well as ultra-small SPIONs or USPIONs (diameter less than 50 nm) [55], where the size of the particle determines biodistribution and clearance from the body. Generally, SPIONs tend to interact with the phagocytic cells of the immune system and tend to rapidly make their way to the liver and spleen that are the nodes of the macrophage system [55]. USPIONs due to their small size make their way into the blood stream with a much lower clearance time increasing their chances of reaching tumours in the rest of the body. Further, systems that have higher saturation magnetization M_S than iron oxide (including Fe-, Mn-, Co-, Ni-based nanoparticles and Dy^{3+} chelates) [54–58] are of interest, since the particle stray field and hence the effect on T_2* scales with the magnetization [59]. However, contrast agents that shorten T_2* result in a reduced signal intensity can be confused for other pathogenic conditions, such as blood clots, and may reduce the signal intensity in

neighbouring tissue resulting in reduced resolution for diagnosis [55]. Reference [55] provides a thorough overview of nanoparticle design for MRI contrast and will be of relevance to the reader.

15.1.1.2 Magnetic Particle Imaging

While MRI had its origins in the 1970s [60], the concept of magnetic particle imaging (MPI) is relatively recent. It was demonstrated in 2005 by Gleich and Weizenecker [23]. Core to this imaging technique is the use of SPIONs as tracers (*not* contrast agents) due to their zero magnetization remanent state, and their nonlinear, saturating magnetization response in an applied field [61–63].

In the presence of a driving alternating applied field at a specific frequency termed the modulation field, the magnetization response of SPIONs is time-dependent and contains both the frequency of the driving field, but also contains higher harmonics. If a strong saturating static field is also applied to the SPIONs, then they remain saturated despite the presence of the alternating field and the generation of the higher harmonics in their magnetization response with time is suppressed. If the spatial configuration of the static field is such that it has a zero (or low) field at its centre and higher fields at the edges, then any SPIONs in the centre of this field retain their higher harmonics in conjunction with the driving field, whereas the SPIONs in the high static field region lose their higher harmonic responses. This is known as the application of a "selection field". MPI thus works by scanning the position of the field-free point (FFP) in the selection field throughout a sample volume containing SPIONs. By mapping the suppression of the higher harmonics of the SPIONs, a tomographic image of the sample volume is generated (Fig. 15.2).

This imaging modality is of extreme interest in the biomedical space. The magnetization response of the SPIONs is the sole contribution to the signal in this technique (hence "tracers"), and it is not confounded with artefacts related to proton relaxation. Further, the higher magnetization and much shorter relaxation times of SPIONs in MPI compared to protons in a 1.5 T applied field means MPI has comparatively extremely high temporal resolution [64] and higher signal to noise than MRI [65]. Further, MPI systems do not need to necessarily be as large as MRI systems and offer flexibility in their design for use [66]. MPI is thus a technique that is of extremely high interest, particularly for cardiovascular diagnostics, tissue perfusion and vascular anomalies, as well as situations where the use of standard MRI contrast agents is not possible from a toxicology perspective such as in patients with compromised renal function [52]. MPI has advanced rapidly since its conception because of its huge potential in the imaging space, and [67–69] will provide the reader with a more detailed overview on MPI in its current state.

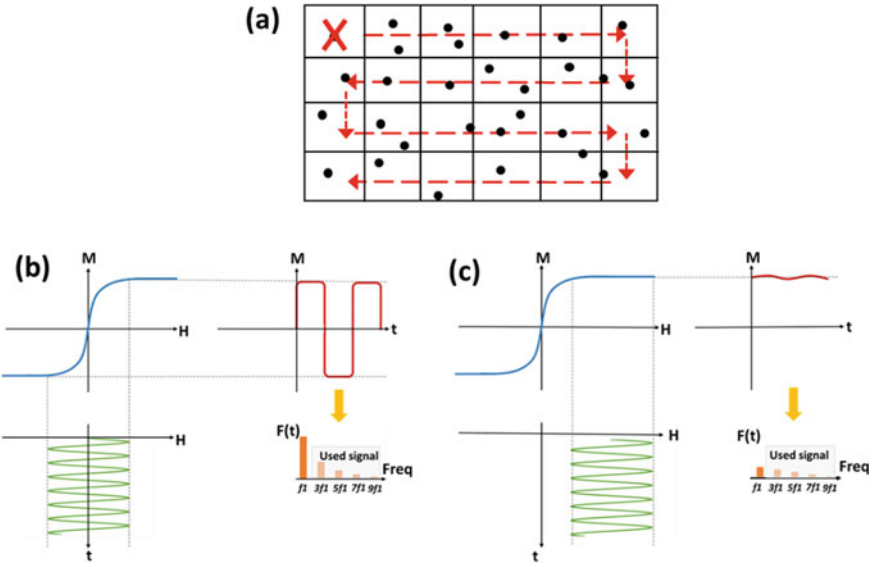

Fig. 15.2 **a** An FFP is scanned through a volume of material containing tracer particles. **b** The magnetization response of particles to the driving field (green) inside the FFP contains higher harmonics. **c** Outside the FFP the higher harmonics are suppressed allowing for tracer mapping as the FFP is scanned over the volume.

15.1.1.3 Magnetic Fluid Hyperthermia

In contrast to the imaging techniques discussed above where diagnostics is the main biomedical focus, magnetic particle hyperthermia is a therapy focussed discipline [29]. Hyperthermia utilizes the energy loss modes available to magnetic nanoparticles in an alternating magnetic field to generate heat in the environment containing the particles. The loss modes that are generally considered are hysteresis losses, Néel (particle magnetization relaxation) and Brown relaxation (particle orientation relaxation) losses, and viscous frictional losses arising from interactions with the fluid during Brown relaxation [70]. The heat generated from these losses is generally lumped into one single figure of merit termed the specific loss power or SLP (termed specific absorption rate or SAR historically). The SLP is defined as the thermal power dissipated per unit mass (typically per gram) of the magnetic material [25, 71].

Magnetic particle hyperthermia is typically conducted at a frequency of 0.05–1.2 MHz and a field amplitude of 0–15 kA/m [8]. The three loss mechanisms are size-dependent, and hence a consideration of magnetic core and hydrodynamic volume are important for evaluating the SLP of a given SPION formulation. Brown and Néel relaxation mechanisms (or a combination of the two) are more relevant for small particles (below the 10 nm range for SPIONs) [70]. Between 10–15 nm, the frequency of the applied field is too high to allow for susceptibility losses, and magnetic switching begins to occur in a coercive manner [70, 70]. This leads to hysteretic losses from

the nanoparticles that are moving away from the superparamagnetic regime. In the 20 nm and above range for iron oxide nanoparticles, the dominant heating process is frictional losses with the fluid due to stirring and the particles are no longer superparamagnetic. This is because the magnetic moment of the larger particles cannot be switched by the field magnitude typically used for hyperthermia [70]. The combination of multiple heating mechanisms, the finite size distribution in nanoparticle formulations [72] and effects such as anisotropy distributions [73–75] and interparticle dipolar interactions [75, 76] has made a comprehensive theoretical model of heat losses in magnetic particle systems quite elusive.

15.1.1.4 Mechanical Actuation

While initial work by F. Crick et al. used magnetic nanoparticles to investigate the microrheology of cell cytoplasm [77], the field has progressed to the point where functionalized blocked magnetic nanoparticles have been attached to individual integrin receptors on the cell membrane. Using a rotating magnetic field, the blocked particles applied torque to the cell membrane providing insight into the mechanical properties of the cytoskeleton [78]. Beyond providing a means to probe mechanical properties, the mechanical actuation of cells via membrane receptors can have significant downstream consequences [79], going as far as to influence gene transcription within the cell [80]. The reader will find [35] that provides a thorough overview of mechanical actuation techniques for cell behavioural modification.

There is also interest in mechanical actuation of cells from a clinical perspective. An area of interest is the directed mediation of mesenchymal stem cell (MSC) differentiation. MSCs differentiate into the various skeletal tissue structures and are a very relevant cell type for tissue engineering and regeneration to grow replacement tissue for a patient. The mechanical loading the cells experience is crucial to the differentiation process [81–83]. Using magnetic nanoparticles to condition cells allows for the mechanical stimulation of cells without a three-dimensional tissue scaffold which is important for the tissue engineering post the culture process [82].

Since mechanical forces can stimulate cells, the forces and torques they exert can also be used to destroy cells by damaging the cytoskeleton [84] or cellular components [85]. There has been work on using iron oxide nanoparticles to destroy cancer cells, where spherical- and rod-shaped iron oxide nanoparticles in an oscillating field have been shown to destroy human cervical cancer cells in vitro [84]. This field, however, has recently received significant attention when highly effective glioblastoma cell killing was demonstrated using a new class of magnetic particle [36]—lithographically defined micro- and nanoparticles which will be discussed further on in this chapter.

15.1.1.5 Biosensing

The sensing of biological analytes is at the core of clinical diagnostics. Magnetic nanoparticles typically used in the biosensing space are iron oxide based, either in core shell structures or functionalized for stability in solution [86]. There are a variety of sensing device architectures for magnetic particles [30, 33, 34, 87–91] but the primary architecture of interest has been magnetoresistance-based devices [92]. An example of such a system would be a giant magnetoresistance (GMR) or spin valve sensor-based assay [32, 93–96]. These are extremely sensitive magnetic field sensors, and here the detection of the analyte is determined by the presence of the stray field of a magnetic nanoparticle near the surface of the sensor. The localization of the nanoparticle on the sensor occurs by specific binding events between biomolecules such as antibody–antigen binding or complementary nucleic acid sequences [93, 97, 98], where the sensor and nanoparticle are both functionalized with the appropriate biomolecule. Magnetic approaches may be the most relevant for assays in biological samples that do not allow for standard optical detection techniques such as fluorescence. Line-of-sight considerations are generally eliminated with magnetic signals and as such magnetic nanoparticle-based assays may be relevant for sensing molecules directly in fluids such as blood [98]. References [82, 88, 89] and [91] provide a broader review of sensing device architectures and nanoparticle formulations in this space (Fig. 15.3).

15.2 Lithographically Defined Particles

Solution suspended lithographically defined magnetic micro- and nanodiscs are a relatively recent development [36, 99–102]. They have emerged because of the interest in transferring the knowledge gained in the fabrication of magnetic memory and logic devices to the biotechnology field. Lithographically defined particles are planar in shape and are generally in the range of 200 nm–2 μm in planar dimensions and 10–200 nm in thickness.

These microdiscs are fabricated with standard lithographic techniques, where most generally a magnetic thin film is grown via physical vapour deposition on patterned photoresist that is spun cast on a silicon wafer. The photoresist is then dissolved and the structures atop the resist are lifted off into solution. The control of magnetic thin-film growth allows for magnetic properties that can be engineered to extreme precision, with resolutions for individual layer thicknesses in the sub-nm range.

The primary challenge with lithographic microdiscs is ensuring a zero remanent magnetization state since they are far too large to be superparamagnetic in nature, and their stray fields are easily sufficient to drive strong magnetic agglomeration. There are two primary approaches used to create microdiscs that do not agglomerate.

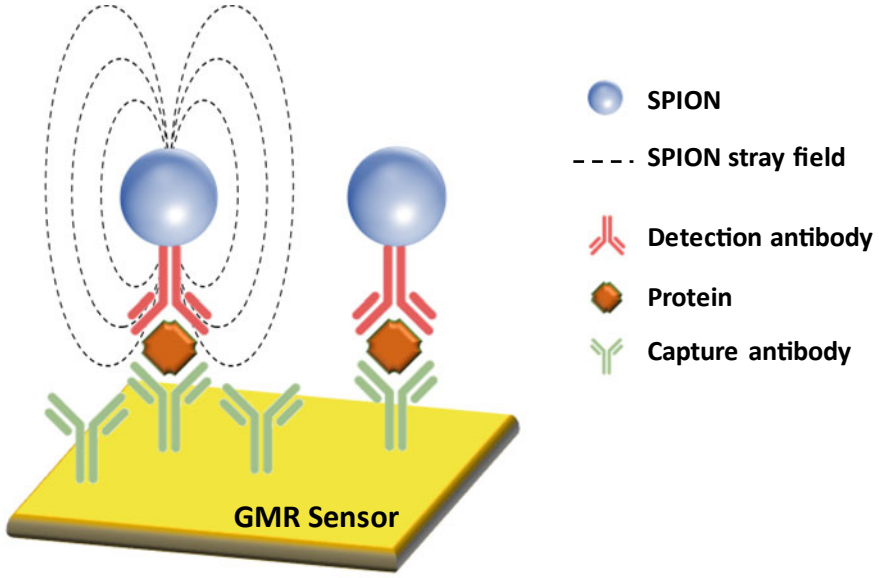

Fig. 15.3 A schematic immunoassay utilizing SPIONs and a GMR type sensor. The sensor top surface is biofunctionalized with a capture antibody. The sample solution containing the protein of interest is poured over the sensor, allowing the protein to be captured by the capture antibody. The sensor surface is then washed and a detection reagent consisting of a complementary detection antibody attached to a SPION is used to confirm the presence of the analyte. Binding of the detection antibody is confirmed by a resistance change in the sensor caused by the stray field of the SPION

The first approach uses magnetically soft materials magnetized in the plane of the particle with weak intrinsic in-plane anisotropy and a symmetric planar shape minimizing in-plane configurational anisotropy [103]. For circular disc configurations in the 200 nm–2 μm diameter range and thicknesses ranging from approximately 10–60 nm (aspect ratios of thickness/diameter typically ranging from 4–40) [104–106], a magnetic flux closure state may be exhibited at remanence known as a magnetic vortex. In such a configuration, the magnetization vector of the disc remains parallel to the nearest disc edge at all points.

The second approach makes use of Ruderman-Kittel-Kasuya-Yoshida (RKKY) [107–109] coupling between adjacent magnetic layers in a multilayer thin film. A phenomenon originally of interest in magnetic memory and logic elements [110–112], it has been of great interest in the space of lithographically fabricated microdiscs. In RKKY coupled systems, two adjacent magnetic layers may be coupled either ferromagnetically or antiferromagnetically (AF) [113, 114] depending on the thickness and composition of the interlayer separating the magnetic layers [115, 116]. A typical example of an RKKY coupling interlayer that can be sandwiched between two magnetic layers is 0.5–1 nm of Ru [116, 117]. When the thickness of the interlayer is tuned to lie in the AF regime, the two magnetic layers lie antiparallel (AP) to each other in the absence of a magnetic field. This AP configuration arising from the

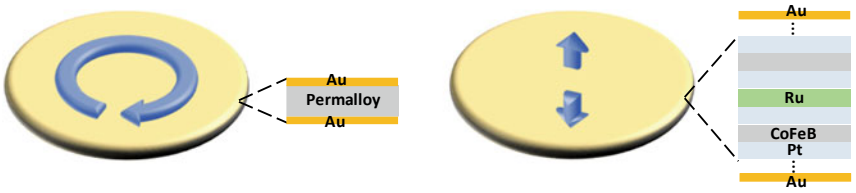

Fig. 15.4 Schematic of two types of microdiscs. The permalloy vortex microdisc (left) has a flux closure magnetization state to ensure a net zero remanent state. The out-of-plane magnetized microdisc (right) utilizes a heterostructure of CoFeB/Pt (for example) to achieve a magnetization perpendicular to the plane of the disc. The Ru interlayer creates an AP remanent state. Both microdiscs are capped with Au for biofunctionalization. The blue arrows denote the magnetization vectors of the magnetic layers in expanded views

AF coupling causes the thin film to have a net zero magnetization at remanence. AF RKKY coupling has been used to create microdiscs with the remanent AP configuration in in-plane magnetic layers (both with and without the vortex configuration) [118, 119], as well as in microdiscs based on perpendicularly magnetized [120–123] magnetic layers [101, 124, 125] (Fig. 15.4).

15.2.1 Applications

15.2.1.1 Mechanical Actuation

Solution suspended lithographically defined microdiscs have been used almost solely for the mechanical destruction of cancer cells, the original application for which they were conceived [36]. The high anisotropy of magnetic thin films translates to the generation of extremely high magnetic torques that are effectively transduced by the planar microdiscs themselves.

Initial work in this space used 2 μm vortex microdiscs in an oscillating magnetic field to destroy glioblastoma cells in vitro [36]. More recently, there has also been interest in using microdiscs fabricated from perpendicularly magnetized thin films for mechanical actuation [101, 124–127]. The mechanical actuation of micro- and nanodiscs structures has been shown to cause significant cell death both in vitro [36, 125] and in vivo [127] and has also been demonstrated in drug delivery-type systems where the actuation can trigger release of a therapeutic [126, 128, 129]. Recent work has been focussed on elucidating the most efficient systems for torque transduction from an applied field, and how that affects the therapeutic efficacy of the particles in a biological system [125].

15.3 Case Studies

15.3.1 Exploring the Potential of MPI In Vivo for the First Time

The first in vivo demonstration of MPI [130] as an imaging modality for cancer detection is of great interest to the field of nanoparticle magnetism. With potential as a high resolution, high sensitivity, safe, and cheap medical imaging technique, MPI is expected to be a field of both commercial and research interest in the biomedical space in the coming decade. The technique is presently capable of imaging ngs of Fe tracer in the form of SPIONs which can correspond to volume of a few hundred cells [131]. Since there is no signal attenuation, and no signal from surrounding tissue, the extremely high contrast technique allows for the visualization of tissue perfusion with resolution potentially down to hundreds of microns [130].

This in vivo study imaged a new SPION-based tracer injected into rats bearing breast cancer tumours. The biodistribution of the tracer was tracked over 6 days providing excellent insight into the behaviour of the tracer for MPI, as well as highlighting the strengths of the technique very effectively.

The LS-008 SPION formulation used for this study was developed by Lodespin Labs has been optimized in other work [132]. The nanoparticles consist of monodisperse oleic acid capped SPION cores around 25 nm that are then coated with poly(maleic anhydride-alt-1-octadecene) (PMAO)—polyethylene glycol (PEG) polymer chains for colloidal stability. This formulation was found to be stable in the high salt concentrations that are found physiologically and that often drive nanoparticle aggregation and impair colloidal stability.

The six-day evolution of the biodistribution of the tracer was tracked with MPI in tumour bearing rats. Seven athymic nude rats were prepared with subcutaneous implantation of breast cancer tumours. The tracer was intravenously injected in the tail 4 weeks after the tumour implantation. Three groups were prepared for the experiment. Group A was a high dose group at 15 mg/kg, group B was a low dose group at 5 mg/kg, and the control group C received no tumour and the high dose. No biofunctionalization was used to target the tumour, but instead the study relied on the fact that tumours preferentially accumulate nanoparticles because of their leakier vasculature than regular tissue, known as the enhanced permeability and retention (EPR) effect [133]. In fact, the study could directly observe the EPR effect and the dynamics of the tracer accumulation in the tumour. An initial enhancement in signal was observed at the edges of the tumour, followed by accumulation, and then the tracer was cleared over the course of 4–6 days (Fig. 15.5).

The quantitative nature of MPI (via a calibration sample) meant that the study could track the amount of tracer in the various organs over time. The pharmacokinetics of the tracer was modelled by a two-compartment method, the blood pool and the tumour. The model fits the experimental results for both the high dose and low-dose group which allowed tracer distribution to be quantified directly from the MPI signal intensity.

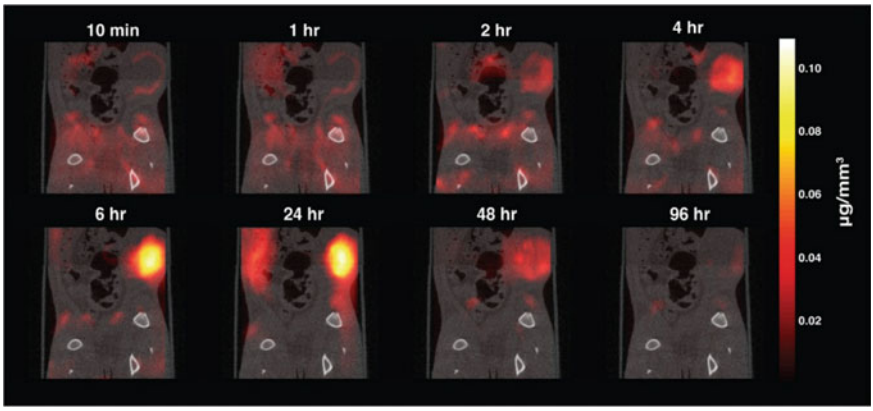

Fig. 15.5 Tracer dynamics observed via MPI for an individual in the high-dose group of rats. Slices through the MPI volume are overlaid with a computed tomography (CT) scan for visualization. The high contrast afforded by the tracer clearly shows three phases of the tracer interaction with the tumour—initial rim enhancement is observed in 10 min, after which the tracer accumulates in the tumour over the course of 24 h, and is subsequently cleared in the next 72 h. Reprinted with permission from Yu et al. [130]. Copyright 2017 American Chemical Society

This study demonstrated the extremely high signal to noise, a factor of 50 here, of which MPI is capable. Further, the high resolution of the technique allowed it to directly observe specific characteristics of the EPR effect, as well as accurately characterize the pharmacokinetics of the tracer. Next steps in this area will be to target tumours actively instead of passively through the EPR mechanism as this may not work with all tumour types. Other exciting prospects will include the combined use of the tracer as a hyperthermia therapy or drug delivery trigger, allowing the tracking of the tumour mass with the ongoing therapy. This two-pronged diagnostic-therapeutic approach could have strong implications in clinical oncology and the development of nanoparticle tracers with characteristics that optimize the efficacy of these two modalities is crucial going forward.

15.3.2 Fuller Treatments of Hyperthermia in Nanoparticle Systems

Moving towards an exploration of all the factors that contribute to the SLP for nanoparticles is necessary to both maximize, and get a better understanding of heat generation for hyperthermia applications. In the work in [134], the authors compare iron oxide nanospheres and nanocubes of 20 nm in diameter (or side length) for their heat generation efficacy. Focussed on magnetic nanoparticles in the single domain regime above the superparamagnetic limit, the work considers the effect

of differences in anisotropy, the presence of interparticle interactions and shape on hyperthermia efficiency.

Inspired by work into bacterial magnetosomes [135], this study demonstrates through experiment the effect of shape and nanoparticle concentration on the SLP and also looks to numerical calculations of the hysteresis loops of the different particle types to draw connections between the structural and magnetic properties of each particle type, and the measured hyperthermia results.

Focussing first on establishing well-characterized nanoparticle formulations as the core of this study, the team fabricated iron oxide nanocubes of 20 and 40 nm in size, as well as nanospheres of 20 nm in size. The different shaped nanoparticles have the same crystal structure (as characterized by transmission electron microscopy (TEM)) and the same size, and the two different sizes of nanocubes allow for a comparison of the effect of size while keeping the shape constant.

The interparticle interaction of the nanocubes is clear in the formation of chain-like aggregates verified by TEM imaging, even in the absence of an applied magnetic field. The effect of these aggregates may seem evident in the concentration dependence of the SLP for both the 20 and 40 nm nanocubes, as well as in the plateauing of the field-cooled curves for the SLP measurements which is not expected for a system of non-interacting particles [134]. Since the SLP decreases with concentration, it seems to suggest from this study that minimizing the interparticle interactions may be of benefit. It was also found via dynamic light scattering measurements that the nanocubes self-assembled into chain-like structures at remanence while the nanospheres did not, showing the importance of shape in interparticle interactions. A curious point of note, however, is that in the simulations conducted it was shown that the SLP appears to monotonically increase with increasing chain length up to ten particles, which would be expected to occur in the samples of higher concentration. Why then does the SAR not similarly increase in the samples where longer chains of particles are to be expected? It may perhaps be the case that minimal ordering on the scale of simple short chains is desirable, but at high concentrations interactions between chains may lead to large clusters that reduce SLP efficiency. A better understanding of the effect of such interparticle interactions is clinically relevant because of the localization of a high dose of nanoparticles in a tumour mass for therapy.

The 20 nm nanocubes were then compared to 20 nm nanospheres, and it was found that there was a 20% increase in the SAR compared to the spheres both experimentally, and this quite closely matched Monte-Carlo simulations of the SAR of the two systems that considered dipolar interactions. The nanocubes were estimated to have an anisotropy approximately 25% higher than the nanospheres at room temperature accounting for dipolar interactions. The higher anisotropy was attributed primarily to the higher surface area of the cubic particles that leads to a higher surface anisotropy contribution since exchange bias effects were shown to be non-existent and a homogenous oxide composition was assumed.

Tuning the shape of nanoparticles thus can have a significant effect on their effectiveness in hyperthermia applications. However, this work highlights some interesting questions about interparticle interactions and their effect on the SAR. Aggregates of particles in chains, for example, have an anisotropy that can be assigned to the entire

chain in addition to the magnetic anisotropy of the individual particle. A thorough understanding of the effect of these dipolar interactions on the SLP and in which regimes they are desirable is needed [136–139].

15.3.3 The Top-Down Engineering of Application Specific Nanoparticles

Lithographically defined microdiscs made from permalloy were shown to be effective at triggering apoptotic cell death in glioblastoma cells in vitro [36] which sparked investigation into the mechanical destruction of cancer cells as a viable cancer therapy. The study featured here [125] began with the hypothesis that the permalloy vortex magnetic configuration was not the most efficient method of torque generation from an applied field, and that magnetic microdiscs with a strong uniaxial anisotropy are more desirable for this application.

Mechanical actuation of magnetic particles in an applied field is dictated largely by the magnetic anisotropy of the particle. The magnetic anisotropy can be thought of as a measure of how strongly the magnetization vector of the particle is linked to its mechanical structure. Optimizing the actuation of magnetic particles for such an application involves engineering its magnetic anisotropy to best fit the type of applied field being used.

Lithographically defined microdiscs are based on thin-film magnetic systems and may have the easy magnetic axis in the plane of the film, or out of the plane of the film. The permalloy vortex is a special case of the in-plane system, where the shape constraints from patterning and the inherently soft material lead to a magnetic system with an easy plane of magnetization (the plane of the microdisc). When a field is applied in the plane of the microdisc the vortex core is displaced resulting in a net magnetization in the direction of the applied field, and this is achieved equally "easily" in any direction in the plane of the disc. Perpendicular magnetic thin films are constructed by alternating layers of a magnetic material (CoFeB) with a heavy metal (Pt) in a multilayer heterostructure. The out-of-plane magnetization is driven by spin–orbit coupling at the CoFeB/Pt interface [120–123]. The perpendicular microdiscs achieve a net zero remanent state by utilizing RKKY AF coupling between adjacent magnetic layers in the multilayer stack. Both sets of discs in this study were 2 μm in diameter. The permalloy vortex discs were 60 nm in permalloy thickness with 5 nm gold caps, and the perpendicular microdisc contained a total of 21.6 nm of CoFeB dispersed in a multilayer heterostructure approximately 110 nm in thickness with 5 nm gold caps. The vortex microdisc thus has a higher magnetic moment than the perpendicular microdiscs, with an easy plane of magnetization as opposed to an easy axis. It should be noted that the hard axis saturation field for the vortex microdiscs was approximately 1 T, and the effective hard axis anisotropy field for the perpendicular particles (once the RKKY coupling is accounted for) was approximately 0.5 T.

Both discs were used to mechanically disrupt glioblastoma cells in vitro, under an applied rotating field of 1 T at 20 Hz for 60 s. This was carried out by incubating the cells with the microdiscs for 24 h which led to the internalization of the microdiscs by the cells. They were then exposed to the magnetic field treatment, and it was found that the perpendicular microdiscs demonstrated approximately 60% cell killing, whereas the vortex microdiscs displayed just 12% cell killing. To understand the large difference in cell killing efficiency, the difference in the magnitude of the magnetic torque and the symmetry of the anisotropy between the two particles was considered.

The study simulated the torque as a function of field angle using a Stoner-Wohlfarth-like model, and compared this to experimental measurements of the magnetization angle as a function of field angle. Both the simulation and experimental results estimated the peak torque of approximately 75 pNm for the vortex microdiscs, and approximately 20 pNm for the perpendicular microdiscs. The difference in peak torque is due to the difference in magnetic moment and anisotropy fields between the two microdiscs. Thus, the magnitude of the torque did not provide an explanation for the difference in performance between the two types of particles since the vortex microdiscs exerted higher peak torques (Fig. 15.6).

It was noted that the symmetry of the anisotropy is the cruci6al difference between the two particles. With a rotating magnetic field, a particle with an easy plane of magnetization will first align its easy plane to the plane of the applied field. The magnetization will then rotate in the plane of the particle without transducing any mechanical torque from the field. The microdisc with the easy magnetization axis,

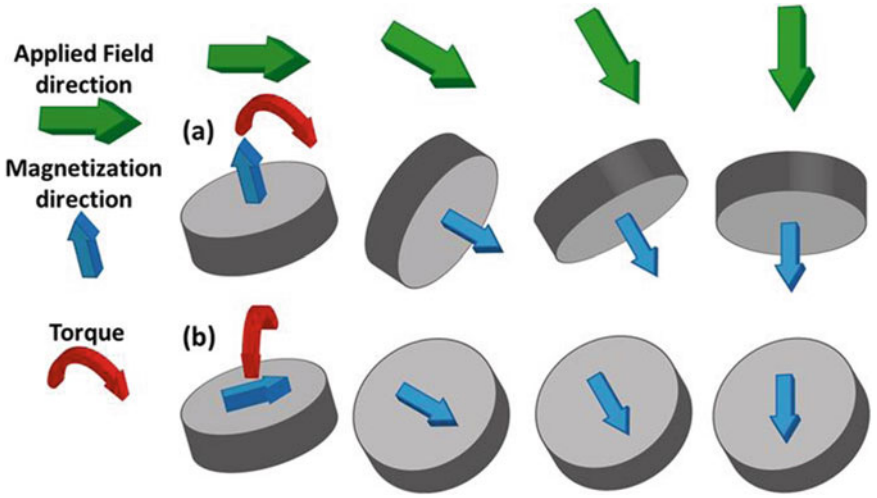

Fig. 15.6 A schematic showing the importance of considering the symmetry of anisotropy in relation to the applied field configuration for mechanical actuation. The magnetization direction and torques on **a** perpendicular particles (top row) and **b** permalloy vortex particles (bottom row) under an applied rotating field. Figure reproduced from [125] with permission

however, will continuously mechanically rotate to align its magnetization with the applied field transducing torque over the entire field duration. Over even the 60 s field duration this proved to be enough to result in a 50% difference in cell killing capability between the two sets of particles. This study clearly highlighted the need to engineer magnetic particles to their application to ensure maximum efficiency. Lithographic techniques offer great precision in this regard and are expected to be of significant interest for the fabrication of magnetic micro- and nanoparticles for biotechnology applications.

15.3.4 Magnetically Driven Labs-On-Chips

The transport of magnetic beads using either domain walls [140] or periodic magnetic elements [141] is an interesting prospect technologically and may offer a new take on lab-on-chip processes where the analyte of interest is not transported by fluid flow as in microfluidics, but via the motion of magnetic beads. The study here [142] demonstrates an architecture of patterned permalloy nanotracks on a Si chip that creates a magnetic domain wall routing network capable of transporting magnetic beads along paths selected by the application of external fields. This has exciting implications for more complex operations such as dynamic sorting of magnetic particles allowing for intricate downstream processing and sensing.

Magnetic domain walls are localized sources of stray field capable of trapping superparamagnetic beads with forces in the range of hundreds of pN [143–146]. Domain walls, and hence the particles they trap, may be moved in micro- and nanowire structures with an applied field at speeds approaching 1 mm/s [140]. A permalloy curvilinear nanotrack was fabricated consisting of semi-circular links, with track width of 800 nm, thickness of 40 nm and an outer diameter of 20 μm for the semi-circular links. A junction was created that spits the track into two paths. This study focussed on vortex-type domain walls [147], a magnetic texture analogous to the vortex flux closure state in a patterned microdisc. A vortex domain wall exists in thin magnetic strips where two in-plane domains of the opposite magnetization direction meet. At this intersection between the two domains, the domain wall forms with a magnetic vortex core in the centre of the wall, and a chirality given by the direction that the magnetization rotates about the core of the wall [148]. The domain wall can be formed in a head-to-head or tail-to-tail configuration according to the direction of the domains in the magnetic strip, and these two configurations may be thought of as having opposite signs, and their stray fields (pointing out of the plane of the track) are of opposite sign as well.

The vortex domain walls in this study are moved in the permalloy nanotrack by a rotating magnetic field of the appropriate rotational direction in the plane of the track. As the domain wall is moved through the junction, it splits and creates two domain walls in each of the new paths, one of the same sign and one of the opposite sign. The crucial point of this work shows that since the domain wall splits into two domain walls of the opposite sign, a field pulse applied out of the plane of the system

is additive for the stray field of one of the domain wall configurations and subtractive for the other. This creates a selection mechanism for the bead as it approaches the junction that is reminiscent of a train switching tracks. The bead is driven to the path with the domain wall that has had its field enhanced at the junction as determined by the sign of the out of plane field pulse.

This selection process is simulated in a model track junction of permalloy 100 nm wide, 60 nm thick, and with a 2 μm outer diameter. An in-plane rotating field of 625 Oe was simulated to drive the domain wall motion, and a ±250 Oe out of plane field was used to create the asymmetric magnetostatic potential energy surface that the bead observes as it exits the junction. Experimentally this process was demonstrated on a series of 2.8 μm beads going through a junction in the fabricated track described above, where the bead switching to path 2 was looked at under various conditions. The out-of-plane fields ranged from −150 to +150 Oe. It was found that the bead does not switch to path 2 if its domain wall stray field is diminished by the applied field which agrees with the simulated result. When the applied field is additive to the domain wall stray field in path 2, the bead only switches to path 2 where the applied filed pulse is above approximately 57 Oe. This minimum magnitude of applied field necessary for switching paths is interesting. It shows that the magnetostatic potential energy surface the bead experiences needs to be modified by a significant external field to drive path switching. It was explained that this is perhaps due to differences in domain wall depinning in the two paths as the domain wall goes through the junction requiring some minimum field magnitude to remove the inherent bias to the bead motion.

This study takes the demonstration one step further by experimentally demonstrating that beads of different sizes can be sorted based on this technique since the potential energy well of interaction of each bead is modified by its magnetic moment. Each bead size thus has different threshold out-of-plane field pulses necessary to switch it to path 2 in the system. Populations of 2.8 and 5.8 μm beads were robustly sorted through a junction using the appropriate out-of-plane fields. If the beads were functionalized to capture different bioanalytes, for example, this sorting mechanism would allow for separation of these analytes, an important step towards multiplexed detection. This study showed a simple but powerful method to transport and sort magnetic beads on a silicon chip. This is an exciting route forward for lab-on-chip-type applications driven largely by magnetic forces and torques and potentially getting around the challenges associated with microfluidic systems [149] (Fig. 15.7).

15.4 Future Perspectives

The fundamental challenge for materials developed for clinical techniques is in achieving the desired materials performance within the required bounds of toxicity that are defined by any in vivo application. Iron oxide-based nanoparticles still form the mainstay of magnetic nanoparticles relevant for this field particularly

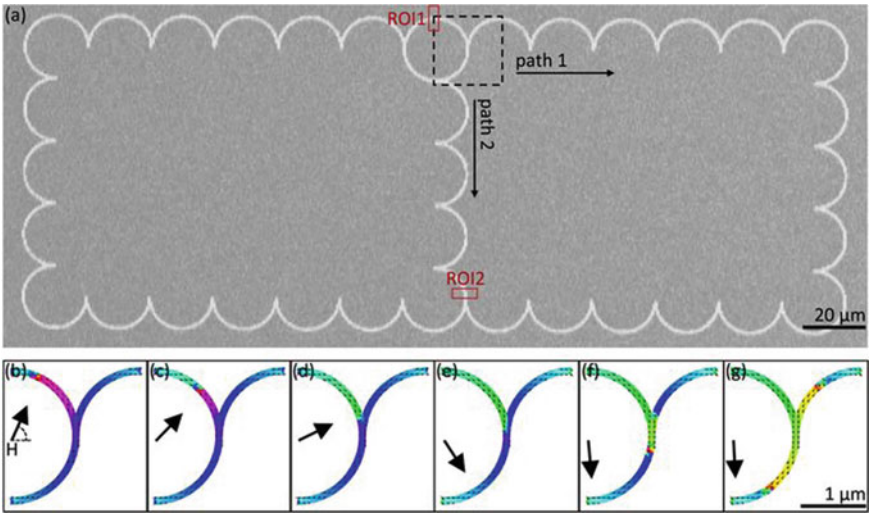

Fig. 15.7 Magnetic nanotrack configuration used to transport magnetic beads with domain walls and simulations of domain wall motion. **a** An optical image of the curvilinear permalloy track composed of 20 µm outer diameter, 800 nm wide, 40 nm thick linked semi-circular segments. The dashed square shows the micromagnetically simulated junction region consisting of a full circle that links two independent paths to an incoming track. **b–g** Evolution of the simulated magnetization configuration in junction region with the rotation of an applied magnetic field (black arrow) in the plane of the track. As the applied in-plane field is rotated in time, a head-to-head domain wall enters the junction, and two domain walls, one head-to-head and one tail-to-tail, exit the junction, one on each path. Figure reproduced from [142] with permission

because they are minimally toxic. Working within these limits, significant progress has been made in the development of iron oxide nanoparticle synthesis that are effective for hyperthermia or imaging applications [150, 151]. The pharmacokinetics and biodistribution of the nanoparticles are also important once they meet the toxicology requirements [152]. Here, size and functional coatings and encapsulations are crucial in ensuring that the nanoparticles remain in the body for long enough to be relevant as therapeutics or image enhancing agents [153]. The optimization of nanoparticle formulations for biostability and minimal toxicity will continue to be a challenge as new nanoparticle systems are developed with better magnetic properties.

For MRI imaging, an area of extreme interest is a dual-mode contrast agent, where both T_1 and T_2* imaging modes may be enhanced and used simultaneously with the same probe [55, 154]. Work in this direction has thus far focussed on core–shell-type nanoparticle structures with a transition metal-based core and a Gd-based shell [154–158]. The Gd shell is in direct contact with the liquid to ensure that the T_1 contrast agent can operate on the short length scale (in "direct contact" with the hydrogen atoms), and the superparamagnetic core is still able to influence the T_2* relaxation process via the stray magnetic field generated [55]. The development of a successful, high-performance, dual-mode probe would be a paradigm shift in the MRI field and work in this area is worthy of attention.

In the imaging space, optimizing SPIONs for the MPI field is an extremely relevant challenge with significant expected impact in the next decade. The performance of SPIONs as MPI tracers is generally evaluated by a combination of the Langevin theory of paramagnetism and understanding the relaxation processes for a magnetized nanoparticle [159, 160]. Magnetic nanoparticles typically consist of a magnetic centre and a coating of a capping polymer or organic molecules. Particles with a larger core have a higher magnetic moment and generally produce higher signal increasing imaging sensitivity. As particles get larger, however, their relaxation time (typically dominated by Brownian processes in MPI) increases [161]. This affects spatial resolution since the particle response to the FFP should be as near to instantaneous as possible to allow for the detection of the higher-order harmonics in the magnetization response to the modulation field. Typically, for a given applied field configuration, the goal is to maximize the size of the SPIONs until particle relaxation begins to impede spatial resolution. The polydispersity of SPION formulations can also have a large impact on MPI performance [160] since both the Langevin function for the magnetization and the Brownian function for relaxation are strongly dependent on particle size [161]. Particles that are smaller than ideal do not have high enough signals, and particles that are larger have long relaxation times, and so the monodispersity of SPION tracers is crucial to maximize MPI signal per unit gram of tracer used. Further, since SPIONs are typically fabricated with an encapsulation for stability and Brownian relaxation processes are dependent on the effective hydrodynamic radius, the optimum coating thickness to magnetic core ratio is also a factor of consideration. With MPI performance so closely tied to the quality of the SPION tracers, there is significant potential for concerted SPION development that may be specific to a given diagnostic application. The commercial interest in development of MPI nanoparticle formulations is evident in that Lodespin Labs has been founded around this goal and has already created the first commercial SPION-based tracer dedicated for MPI [132].

From the thermal ablation perspective, there are two overarching goals moving forward. The first is to develop nanoparticle formulations to maximize the SLP, with a minimum figure of merit of 1000 W/g at 100 kHz and 20 mT [162]. This is already significantly higher than the 200–600 W/g obtained from commercially available SPION formulations [133]. The work in this area has moved towards modifying the nanoparticle structure and material composition with a variety of core–shell structures utilizing exchange coupling [28, 131, 163, 164] to massively increase the SLP. Three materials properties that are of importance here are nanoparticles diameter D, anisotropy K, the nanoparticle shape and saturation magnetization M_S. The particularly relevant parameter to tune is the anisotropy of the nanoparticles used [75, 165–167], and it is here that the interfacial coupling between core–shell nanoparticles becomes relevant. By using a hard magnetic core and soft magnetic shell that are magnetically coupled, the anisotropy can be tuned to be close to the theoretically ideal point for maximizing the SLP with values of 1000–4000 W/g [28] demonstrated. With nanoparticle shape and size, optimized values in excess of 10,000 W/g have been observed [167]. Most of this work has focussed on Mn, Zn and Co ferrites which may prove to be challenging with regard to regulatory approval

for clinical deployment. These approaches may feed into novel iron oxide-based nanoparticle development with interesting shape and magnetic structures that could unlock high SAR values while allowing for safe clinical deployment [168, 169]. The second goal for magnetic hyperthermia has been in establishing a general theoretical framework. Strong steps forward have been made by creating theoretical models for the various aspects comprising the whole. This includes modelling hysteresis processes [170, 171], understanding the role of interparticle dipolar interactions on the SLP [136–139, 172, 173], and the role of the anisotropy of magnetic particle aggregates [75, 174]. Developing a theoretical framework that encapsulates the full complexity of hyperthermia processes, along with a strong push towards optimizing nanoparticle fabrication within the toxicity restrictions of an in vivo application is crucial for the commercial future of clinical magnetically driven thermal ablation techniques. It is expected to be unlikely [175] that magnetic particle hyperthermia will in the short term be the silver bullet that entirely replaces the more damaging cancer therapies of chemo and radiotherapy, but it may find applicability in specific instances of cancer treatment [176, 177].

Diagnostics applications that do not require in vivo deployment of magnetic nanoparticles allow more flexibility in particle composition as they are not as restricted by toxicity considerations. This may be of relevance for MR-based sensing techniques where the sensor detects the stray field from a nanoparticle as a positive signal. Here, nanoparticle development may be towards developing techniques that maximize the stray field of the particles while minimizing agglomeration, and developing nanoparticles optimized for detection by MR type sensors may prove worthwhile [96]. With recent interest in the manipulation of magnetic beads on chips using the motion of domain walls or patterned magnetic structures [140–145, 178, 179], there is potentially an alternative to microfluidic-based approaches to biomolecule capture, transport and detection. Combined with optical, electrical or magnetic sensing-based approaches, this is an interesting way forward for nanoparticle techniques in the biosensing space.

In addition to colloidally synthesized magnetic nanoparticles, lithographically defined structures for biotechnology applications have also been discussed here. The attraction of lithographically defined microdiscs is the ability to engineer magnetic particles with a precision that is simply not offered by colloidal chemistry fabrication techniques [99]. By being able to finely tune the size and shape of the discs, as well as the amount of magnetic material, and the strength and orientation of the magnetic anisotropy, local forces and torques may be applied with a high degree of control. This is particularly relevant in cell manipulation for downstream responses as cellular processes may be triggered by mechanical stimulation. For cancer cell death, for example, torques in the range of aNm may trigger apoptotic cell death [36] via ion channel mediation, a mechanism that does not trigger an inflammatory response in the body and is important for treatments in the brain.

While work thus far has focussed on their use in therapy type applications, it will be worthwhile to explore the potential of lithographically defined particles in lab-on-chip-type systems. A need for the controlled manipulation of magnetic particles on chip may better suit the lower fabrication yields and precisely tunable magnetic

characteristics of magnetic thin-film-based fabrication techniques. While defining the application space where these particles will be the most effective has proved challenging, general insights may be gained by their use since their properties may be conveniently engineered. A thorough exploration of the available existing and potential future applications with regard to these types of particles will be a worthwhile undertaking to best understand where they may be most effectively deployed.

Lithographically defined particles represent systems where the magnetic properties can be extremely accurately tuned but are limited in the volume that they can be fabricated. Colloidal synthesis is on the other end of the spectrum and offers an approach for high volume fabrication of magnetic nanoparticles but is somewhat limited in the precision engineering of the magnetic properties of the particles. As both these techniques evolve further the gap between them is likely to be bridged allowing a broader range of magnetic micro- and nanoparticles that will be exciting for the biomedical field.

Magnetic nanoparticles cover a wide range of applications in the biomedical space, ranging from in vivo imaging and therapy to ex vivo diagnostics. Nanoparticle synthesis and fabrication has continually evolved and opened new areas where these systems offer benefit and insight. It is expected that this community will continue to make strong contributions towards solving the varied and exciting challenges offered by the biomedical space.

References

1. U. Jeong, X. Teng, Y. Wang, H. Yang, Y. Xia, Adv. Mater. **19**, 33 (2007). https://doi.org/10.1002/adma.200600674
2. R. Hao, R. Xing, Z. Xu, Y. Hou, S. Gao, S. Sun, Adv. Mater. **22**, 2729 (2010). https://doi.org/10.1002/adma.201000260
3. T. Neuberger, B. Schöpf, H. Hofmann, M. Hofmann, B. von Rechenberg, J. Magn. Magn. Mater. **293**, 483 (2005). https://doi.org/10.1016/j.jmmm.2005.01.064
4. S. Sun, H. Zeng, J. Am. Chem. Soc. **124**, 8204 (2002). https://doi.org/10.1021/ja026501x
5. S. Laurent, D. Forge, M. Port, A. Roch, C. Robic, L. Vander Elst, R.N. Muller, Chem. Rev. **108**, 2064 (2008). https://doi.org/10.1021/cr068445e
6. A.K. Gupta, M. Gupta, Biomaterials **26**, 3995 (2005). https://doi.org/10.1016/j.biomaterials.2004.10.012
7. L.H. Reddy, J.L. Arias, J. Nicolas, P. Couvreur, Chem. Rev. **112**, 5818 (2012). https://doi.org/10.1021/cr300068p
8. Q.A Pankhurst, J. Connolly, S.K. Jones, J. Dobson, J. Phys. D. Appl. Phys. **36**, R167 (2003). https://doi.org/10.1088/0022-3727/36/13/201
9. M.L. Néel, Ann. Geophys. **5**, 99 (1949). https://doi.org/10.1017/CBO9781107415324.004
10. W.F. Brown, Phys. Rev. **130**, 1677 (1963). https://doi.org/10.1103/PhysRev.130.1677
11. A.-H. Lu, E.L. Salabas, F. Schüth, Angew. Chemie Int. Ed. **46**, 1222 (2007). https://doi.org/10.1002/anie.200602866
12. R.H. Kodama, J. Magn. Magn. Mater. **200**, 359 (1999). https://doi.org/10.1016/S0304-8853(99)00347-9
13. I. Sharifi, H. Shokrollahi, S. Amiri, J. Magn. Magn. Mater. **324**, 903 (2012). https://doi.org/10.1016/j.jmmm.2011.10.017

14. H. Deng, X. Li, Q. Peng, X. Wang, J. Chen, Y. Li, Angew. Chemie Int. Ed. **44**, 2782 (2005). https://doi.org/10.1002/anie.200462551
15. M. Bellusci, C. Aliotta, D. Fiorani, A. La Barbera, F. Padella, D. Peddis, M. Pilloni, D. Secci, J. Nanoparticle Res. **14**, 904 (2012). https://doi.org/10.1007/s11051-012-0904-7
16. D. Peddis, N. Yaacoub, M. Ferretti, A. Martinelli, G. Piccaluga, A. Musinu, C. Cannas, G. Navarra, J.M. Greneche, D. Fiorani, J. Phys. Condens. Matter **23**, 426004 (2011). https://doi.org/10.1088/0953-8984/23/42/426004
17. J. McCarthy, R. Weissleder, Adv. Drug Deliv. Rev. **60**, 1241 (2008). https://doi.org/10.1016/j.addr.2008.03.014
18. Y. Jun, J. Lee, J. Cheon, Angew. Chemie Int. Ed. **47**, 5122 (2008). https://doi.org/10.1002/anie.200701674
19. A. Louie, Chem. Rev. **110**, 3146 (2010). https://doi.org/10.1021/cr9003538
20. Y.-X.J. Wang, S.M. Hussain, G.P. Krestin, Eur. Radiol. **11**, 2319 (2001). https://doi.org/10.1007/s003300100908
21. H. Bin Na, I.C. Song, T. Hyeon, Adv. Mater. **21**, 2133 (2009). https://doi.org/10.1002/adma.200802366.
22. J.W.M. Bulte, D.L. Kraitchman, NMR Biomed. **17**, 484 (2004). https://doi.org/10.1002/nbm.924
23. B. Gleich, J. Weizenecker, Nature **435**, 1214 (2005). https://doi.org/10.1038/nature03808
24. A. Jordan, R. Scholz, K. Maier-Hauff, M. Johannsen, P. Wust, J. Nadobny, H. Schirra, H. Schmidt, S. Deger, S. Loening, W. Lanksch, R. Felix, J. Magn. Magn. Mater. **225**, 118 (2001). https://doi.org/10.1016/S0304-8853(00)01239-7
25. R. Hergt, S. Dutz, R. Müller, M. Zeisberger, J. Phys. Condens. Matter **18**, S2919 (2006). https://doi.org/10.1088/0953-8984/18/38/S26
26. S. Laurent, S. Dutz, U.O. Häfeli, M. Mahmoudi, Adv. Colloid Interface Sci. **166**, 8 (2011). https://doi.org/10.1016/j.cis.2011.04.003
27. C.S.S.R. Kumar, F. Mohammad, Adv. Drug Deliv. Rev. **63**, 789 (2011). https://doi.org/10.1016/j.addr.2011.03.008
28. J.H. Lee, J.T. Jang, J.S. Choi, S.H. Moon, S.H. Noh, J.W. Kim, J.G. Kim, I.S. Kim, K.I. Park, J. Cheon, Nat. Nanotechnol. **6**, 418 (2011). https://doi.org/10.1038/nnano.2011.95
29. A. Jordan, R. Scholz, P. Wust, H. Fähling, R. Felix, J. Magn. Magn. Mater. **201**, 413 (1999). https://doi.org/10.1016/S0304-8853(99)00088-8
30. Y.R. Chemla, H.L. Grossman, Y. Poon, R. McDermott, R. Stevens, M.D. Alper, J. Clarke, Proc. Natl. Acad. Sci. U. S. A. **97**, 14268 (2000). https://doi.org/10.1073/pnas.97.26.14268
31. J.M. Nam, C.S. Thaxton, C.A. Mirkin, Science (80-.) **301**, 1884 (2003). https://doi.org/10.1126/science.1088755
32. D.A. Hall, R.S. Gaster, T. Lin, S.J. Osterfeld, S. Han, B. Murmann, S.X. Wang, Biosens. Bioelectron. **25**, 2051 (2010). https://doi.org/10.1016/j.bios.2010.01.038
33. G. Li, S. Sun, R.J. Wilson, R.L. White, N. Pourmand, S.X. Wang, Sensors Actuators. a Sens. Actuators Phys. **126**, 98 (2006). https://doi.org/10.1016/j.sna.2005.10.001
34. S.X. Wang, G. Li, in IEEE Trans. Magn. 1687–1702 (2008). https://doi.org/10.1109/TMAG.2008.920962.
35. J. Dobson, Nat. Nanotechnol. **3**, 139 (2008). https://doi.org/10.1038/nnano.2008.39
36. D.-H. Kim, E.A Rozhkova, I.V Ulasov, S.D. Bader, T. Rajh, M.S. Lesniak, V. Novosad, Nat. Mater. **9**, 165 (2010). https://doi.org/10.1038/nmat2591
37. F. Bloch, Phys. Rev. **70**, 460 (1946). https://doi.org/10.1103/PhysRev.70.460
38. E.M. Purcell, H.C. Torrey, R.V. Pound, Phys. Rev. **69**, 37 (1946). https://doi.org/10.1103/PhysRev.69.37
39. C.F.G.C. Geraldes, S. Laurent, Contrast Media Mol. Imaging **4**, 1 (2009). https://doi.org/10.1002/cmmi.265
40. R.A. Pooley, Radiographics **25**, 1087 (2005). https://doi.org/10.1148/rg.254055027
41. P.A. Bottomley, C.J. Hardy, R.E. Argersinger, G. Allen Moore, Med. Phys. **14**, 1 (1987). https://doi.org/10.1118/1.596111

42. C.T. Yang, P. Padmanabhan, B.Z. Gulyás, RSC Adv. **6**, 60945 (2016). https://doi.org/10.1039/c6ra07782j
43. G. Marchal, Y. Ni, P. Herijgers, W. Flameng, C. Petré, H. Bosmans, J. Yu, W. Ebert, C.S. Hilger, D. Pfefferer, W. Semmler, A.L. Baert, Eur. Radiol. **6**, 2 (1996). https://doi.org/10.1007/BF00619942
44. H. Bin Na, T. Hyeon, J. Mater. Chem. **19**, 6267 (2009). https://doi.org/10.1039/b902685a
45. S. Flacke, S. Fischer, M.J. Scott, R.J. Fuhrhop, J.S. Allen, M. McLean, P. Winter, G.A. Sicard, P.J. Gaffney, S.A. Wickline, G.M. Lanza, Circulation **104**, 1280 (2001). https://doi.org/10.1161/hc3601.094303
46. R.J. Kim, E.L. Chen, J.A.C. Lima, R.M. Judd, Circulation **94**, 3318 (1996). https://doi.org/10.1161/01.CIR.94.12.3318
47. E. Wiener, M.W. Brechbiel, H. Brothers, R.L. Magin, O.A. Gansow, D.A. Tomalia, P.C. Lauterbur, Magn. Reson. Med. **31**, 1 (1994). https://doi.org/10.1002/mrm.1910310102
48. V. Trubetskoy, Adv. Drug Deliv. Rev. **37**, 81 (1999). https://doi.org/10.1016/S0169-409X(98)00100-8
49. C.H. Reynolds, N. Annan, K. Beshah, J.H. Huber, S.H. Shaber, R.E. Lenkinski, J.A. Wortman, J. Am. Chem. Soc. **122**, 8940 (2000). https://doi.org/10.1021/ja001426g
50. P. Chandran, A. Sasidharan, A. Ashokan, D. Menon, S. Nair, M. Koyakutty, Nanoscale **3**, 4150 (2011). https://doi.org/10.1039/c1nr10591d
51. J. Kukowska-Latallo, Int. J. Nanomedicine **3**, 201 (2008). https://doi.org/10.2147/ijn.s2696
52. Y. Wang, T.K. Alkasab, O. Narin, R.M. Nazarian, R. Kaewlai, J. Kay, H.H. Abujudeh, Int. Braz J Urol **37**, 541 (2011). https://doi.org/10.1590/S1677-55382011000400018
53. T.G. St. Pierre, P.R. Clark, W. Chua-Anusorn, A.J. Fleming, G.P. Jeffrey, J.K. Olynyk, P. Pootrakul, E. Robins, R. Lindeman, Blood **105**, 855 (2005). https://doi.org/10.1182/blood-2004-01-0177
54. Z.R. Stephen, F.M. Kievit, M. Zhang, Mater. Today **14**, 330 (2011). https://doi.org/10.1016/S1369-7021(11)70163-8
55. M.A. Busquets, J. Estelrich, M.J. Sánchez-Martín, Int. J. Nanomedicine **10**, 1727 (2015). https://doi.org/10.2147/IJN.S76501
56. G.K. Das, N.J.J. Johnson, J. Cramen, B. Blasiak, P. Latta, B. Tomanek, F.C.J.M. Van Veggel, J. Phys. Chem. Lett. **3**, 524 (2012). https://doi.org/10.1021/jz201664h
57. H. Yang, C. Zhang, X. Shi, H. Hu, X. Du, Y. Fang, Y. Ma, H. Wu, S. Yang, Biomaterials **31**, 3667 (2010). https://doi.org/10.1016/j.biomaterials.2010.01.055
58. C.G. Hadjipanayis, M.J. Bonder, S. Balakrishnan, X. Wang, H. Mao, G.C. Hadjipanayis, Small **4**, 1925 (2008). https://doi.org/10.1002/smll.200800261
59. Q.L. Vuong, J.F. Berret, J. Fresnais, Y. Gossuin, O. Sandre, Adv. Healthc. Mater. **1**, 502 (2012). https://doi.org/10.1002/adhm.201200078
60. P.C. Lauterbur, Nature **242**, 190 (1973). https://doi.org/10.1038/242190a0
61. A.P. Khandhar, R.M. Ferguson, H. Arami, K.M. Krishnan, Biomaterials **34**, 3837 (2013). https://doi.org/10.1016/j.biomaterials.2013.01.087
62. D. Eberbeck, F. Wiekhorst, S. Wagner, L. Trahms, Appl. Phys. Lett. **98**, 182502 (2011). https://doi.org/10.1063/1.3586776
63. S. Biederer, T. Knopp, T.F. Sattel, K. Lüdtke-Buzug, B. Gleich, J. Weizenecker, J. Borgert, T.M. Buzug, J. Phys. D. Appl. Phys. **42**, 205007 (2009). https://doi.org/10.1088/0022-3727/42/20/205007
64. P.C. Fannin, S.W. Charles, J. Phys. D. Appl. Phys. **22**, 187 (1989). https://doi.org/10.1088/0022-3727/22/1/027
65. P.W. Goodwill, A. Tamrazian, L.R. Croft, C.D. Lu, E.M. Johnson, R. Pidaparthi, R.M. Ferguson, A.P. Khandhar, K.M. Krishnan, S.M. Conolly, Appl. Phys. Lett. **98**, 262502 (2011). https://doi.org/10.1063/1.3604009
66. N. Panagiotopoulos, F. Vogt, J. Barkhausen, T.M. Buzug, R.L. Duschka, K. Lüdtke-Buzug, M. Ahlborg, G. Bringout, C. Debbeler, M. Gräser, C. Kaethner, J. Stelzner, H. Medimagh, J. Haegele, Int. J. Nanomedicine **10**, 3097 (2015). https://doi.org/10.2147/IJN.S70488

67. J. Weizenecker, B. Gleich, J. Rahmer, H. Dahnke, J. Borgert, Phys. Med. Biol. **54**, L1 (2009). https://doi.org/10.1088/0031-9155/54/5/L01
68. R.M. Ferguson, A.P. Khandhar, K.M. Krishnan, J. Appl. Phys. **111**, 07B318 (2012). https://doi.org/10.1063/1.3676053
69. M.H. Pablico-Lansigan, S.F. Situ, A.C.S. Samia, Nanoscale **5**, 4040 (2013). https://doi.org/10.1039/c3nr00544e
70. G. Vallejo-Fernandez, O. Whear, A.G. Roca, S. Hussain, J. Timmis, V. Patel, K. O'Grady, J. Phys. D. Appl. Phys. **46**, 312001 (2013). https://doi.org/10.1088/0022-3727/46/31/312001
71. R. Hergt, R. Hiergeist, M. Zeisberger, G. Glöckl, W. Weitschies, L.P. Ramirez, I. Hilger, W.A. Kaiser, J. Magn. Magn. Mater. **280**, 358 (2004). https://doi.org/10.1016/j.jmmm.2004.03.034
72. R. Hergt, S. Dutz, M. Röder, J. Phys. Condens. Matter **20**, 385214 (2008). https://doi.org/10.1088/0953-8984/20/38/385214
73. A.A. McGhie, C. Marquina, K. O'Grady, G. Vallejo-Fernandez, J. Phys. D. Appl. Phys. **50**, 455003 (2017). https://doi.org/10.1088/1361-6463/aa88ed
74. G. Vallejo-Fernandez, K. O'Grady, Appl. Phys. Lett. **103**, 142417 (2013). https://doi.org/10.1063/1.4824649
75. C.L. Dennis, R. Ivkov, Int. J. Hyperth. **29**, 715 (2013). https://doi.org/10.3109/02656736.2013.836758
76. I.M. Obaidat, B. Issa, Y. Haik, Nanomaterials **5**, 63 (2014). https://doi.org/10.3390/nano5010063
77. F.H.C. Crick, A.F.W. Hughes, Exp. Cell Res. **1**, 37 (1950). https://doi.org/10.1016/0014-4827(50)90048-6
78. N. Wang, J.P. Butler, D.E. Ingber, Science (80-.). **260**, 1124 (1993). https://doi.org/10.1126/science.7684161
79. A. Du Toit, Nat. Rev. Mol. Cell Biol. **14**, 196 (2013). https://doi.org/10.1038/nrm3534
80. C.J. Meyer, F.J. Alenghat, P. Rim, J.H.J. Fong, B. Fabry, D.E. Ingber, Nat. Cell Biol. **2**, 666 (2000). https://doi.org/10.1038/35023621
81. H.A. Benhardt, E.M. Cosgriff-Hernandez, Tissue Eng. Part B Rev. **15**, 467 (2009). https://doi.org/10.1089/ten.teb.2008.0687
82. S.H. Cartmell, J. Dobson, S.B. Verschueren, A.J. El Haj, IEEE Trans. Nanobioscience **1**, 92 (2002). https://doi.org/10.1109/TNB.2002.806945
83. G.R. Kirkham, K.J. Elliot, A. Keramane, D.M. Salter, J.P. Dobson, A.J. El Haj, S.H. Cartmell, IEEE Trans. Nanobioscience **9**, 71 (2010). https://doi.org/10.1109/TNB.2010.2042065
84. D. Cheng, X. Li, G. Zhang, H. Shi, Nanoscale Res. Lett. **9**, 195 (2014). https://doi.org/10.1186/1556-276X-9-195
85. M. Domenech, I. Marrero-Berrios, M. Torres-Lugo, C. Rinaldi, ACS Nano **7**, 5091 (2013). https://doi.org/10.1021/nn4007048
86. T.A.P. Rocha-Santos, TtrAc Trends Anal. Chem. **62**, 28 (2014). https://doi.org/10.1016/j.trac.2014.06.016
87. S.X. Wang, S.Y. Bae, G. Li, S. Sun, R.L. White, J.T. Kemp, C.D. Webb, J. Magn. Magn. Mater. 731–736 (2005). https://doi.org/10.1016/j.jmmm.2005.02.054
88. P.I. Nikitin, P.M. Vetoshko, T.I. Ksenevich, J. Magn. Magn. Mater. **311**, 445 (2007). https://doi.org/10.1016/j.jmmm.2006.10.1180
89. I. Koh, L. Josephson, Sensors **9**, 8130 (2009). https://doi.org/10.3390/s91008130
90. J.B. Haun, T.J. Yoon, H. Lee, R. Weissleder, Wiley Interdiscip. Rev. Nanomedicine. NanoBiotechnology **2**, 291 (2010). https://doi.org/10.1002/wnan.84
91. J. Connolly, T.G. St Pierre, J. Magn. Magn. Mater. **225**, 156 (2001). https://doi.org/10.1016/S0304-8853(00)01245-2
92. G. Lin, D. Makarov, O.G. Schmidt, Lab Chip **17**, 1884 (2017). https://doi.org/10.1039/c7lc00026j
93. S.J. Osterfeld, H. Yu, R.S. Gaster, S. Caramuta, L. Xu, S.J. Han, D.A. Hall, R.J. Wilson, S. Sun, R.L. White, R.W. Davis, N. Pourmand, S.X. Wang, Proc. Natl. Acad. Sci. U. S. A. **105**, 20637 (2008). https://doi.org/10.1073/pnas.0810822105

94. D.L. Graham, H.A. Ferreira, P.P. Freitas, Trends Biotechnol. **22**, 455 (2004). https://doi.org/10.1016/j.tibtech.2004.06.006
95. J. Schotter, P.B. Kamp, A. Becker, A. Pühler, G. Reiss, H. Brückl, Biosens. Bioelectron. **19**, 1149 (2004). https://doi.org/10.1016/j.bios.2003.11.007
96. W. Wang, Y. Wang, L. Tu, Y. Feng, T. Klein, J.-P. Wang, Sci. Rep. **4**, 5716 (2015). https://doi.org/10.1038/srep05716
97. J.R. Lee, C.T. Chan, D. Ruderman, H.Y. Chuang, R.S. Gaster, M. Atallah, P. Mallick, S.W. Lowe, S.S. Gambhir, S.X. Wang, Nano Lett. **17**, 6644 (2017). https://doi.org/10.1021/acs.nanolett.7b02591
98. R.S. Gaster, D.A. Hall, C.H. Nielsen, S.J. Osterfeld, H. Yu, K.E. MacH, R.J. Wilson, B. Murmann, J.C. Liao, S.S. Gambhir, S.X. Wang, Nat. Med. **15**, 1327 (2009). https://doi.org/10.1038/nm.2032
99. E.A. Vitol, V. Novosad, E.A. Rozhkova, Nanomedicine **7**, 1611 (2012). https://doi.org/10.2217/nnm.12.133
100. E.A. Vitol, V. Novosad, E.A. Rozhkova, IEEE Trans. Magn. **48**, 3269 (2012). https://doi.org/10.1109/TMAG.2012.2198209
101. T. Vemulkar, E.N. Welbourne, R. Mansell, D.C.M.C. Petit, R.P. Cowburn, Appl. Phys. Lett. **110**, 042402 (2017). https://doi.org/10.1063/1.4974211
102. W. Hu, R.J. Wilson, A. Koh, A. Fu, A.Z. Faranesh, C.M. Earhart, S.J. Osterfeld, S.J. Han, L. Xu, S. Guccione, R. Sinclair, S.X. Wang, Adv. Mater. **20**, 1479 (2008). https://doi.org/10.1002/adma.200703077
103. R.P. Cowburn, D.K. Koltsov, A.O. Adeyeye, M.E. Welland, 2 (1999)
104. W. Scholz, K.Y. Guslienko, V. Novosad, D. Suess, T. Schrefl, R. Chantrell, J. Fidler, J. Magn. Magn. Mater. **266**, 155 (2003). https://doi.org/10.1016/S0304-8853(03)00466-9
105. K.Y. Guslienko, V. Novosad, Y. Otani, H. Shima, K. Fukamichi, Appl. Phys. Lett. **78**, 3848 (2001). https://doi.org/10.1063/1.1377850
106. K.Y. Guslienko, V. Novosad, Y. Otani, H. Shima, K. Fukamichi, Phys. Rev. B Condens. Matter Mater. Phys. **65**, 244141 (2002). https://doi.org/10.1103/PhysRevB.65.024414
107. T. Kasuya, Prog. Theor. Phys. **16**, 45 (1956)
108. C. Kittel, M.A. Ruderman, Phsyical Rev. **96**, 72 (1954)
109. K. Yosida, Phys. Rev. **106** (1957)
110. J.L. Leal, M.H. Kryder, J. Appl. Phys. **83**, 3720 (1998). https://doi.org/10.1063/1.366597
111. S. Bandiera, R.C. Sousa, Y. Dahmane, C. Ducruet, C. Portemont, V. Baltz, S. Auffret, I.L. Prejbeanu, B. Dieny, I.E.E.E. Magn, Lett. **1**, 3000204 (2010). https://doi.org/10.1109/LMAG.2010.2052238
112. R. Lavrijsen, J.H. Lee, A. Fernández-Pacheco, D.C.M.C. Petit, R. Mansell, R.P. Cowburn, Nature **493**, 647 (2013). https://doi.org/10.1038/nature11733
113. P. Bruno, J. Phys. Condens. Matter **11**, 9403 (1999). https://doi.org/10.1088/0953-8984/11/48/305
114. P. Bruno, C. Chappert, Phys. Rev. Lett. **67**, 1602 (1991)
115. D. Mauri, S.S. Parkin, **44**, 7131 (1991)
116. S.S. Parkin, Phys. Rev. Lett. **67**, 3598 (1991)
117. M. D. Stiles, **2**, 1 (2002).
118. S. Leulmi, H. Joisten, T. Dietsch, C. Iss, M. Morcrette, S. Auffret, P. Sabon, B. Dieny, Appl. Phys. Lett. **103**, 132412 (2013). https://doi.org/10.1063/1.4821854
119. T. Courcier, H. Joisten, P. Sabon, S. Leulmi, T. Dietsch, J. Faure-Vincent, S. Auffret, B. Dieny, Appl. Phys. Lett. **99**, 093107 (2011). https://doi.org/10.1063/1.3633121
120. M.T. Johnson, P.J.H. Bloemen, F.J.A. Den Broeder, J.J. De Vries, Reports. Prog. Phys. **59**, 1409 (1996). https://doi.org/10.1088/0034-4885/59/11/002
121. P. Bruno, Phys. Rev. B **39**, 865 (1989). https://doi.org/10.1103/PhysRevB.39.865
122. G.C. Fletcher, Proc. Phys. Soc. Sect. A **67**, 505 (1954). https://doi.org/10.1088/0370-1298/67/6/303
123. J.H. Van Vleck, Phys. Rev. **52**, 1178 (1937). https://doi.org/10.1103/PhysRev.52.1178

124. T. Vemulkar, R. Mansell, D.C.M.C. Petit, R.P. Cowburn, M.S. Lesniak, Appl. Phys. Lett. **107**, 012403 (2015). https://doi.org/10.1063/1.4926336
125. R. Mansell, T. Vemulkar, D.C.M.C. Petit, Y. Cheng, J. Murphy, M.S. Lesniak, R.P. Cowburn, Sci. Rep. **7**, 4257 (2017). https://doi.org/10.1038/s41598-017-04154-1
126. M.E. Muroski, R.A. Morshed, Y. Cheng, T. Vemulkar, R. Mansell, Y. Han, L. Zhang, K.S. Aboody, R.P. Cowburn, M.S. Lesniak, PLoS ONE **11**, e0145129 (2016). https://doi.org/10.1371/journal.pone.0145129
127. Y. Cheng, M.E. Muroski, D.C.M.C. Petit, R. Mansell, T. Vemulkar, R.A. Morshed, Y. Han, I.V. Balyasnikova, C.M. Horbinski, X. Huang, L. Zhang, R.P. Cowburn, M.S. Lesniak, J. Control. Release **223**, 75 (2016). https://doi.org/10.1016/j.jconrel.2015.12.028
128. Y. Zhang, J. Yu, H.N. Bomba, Y. Zhu, Z. Gu, Chem. Rev. **116**, 12536 (2016). https://doi.org/10.1021/acs.chemrev.6b00369
129. Y. Qiu, S. Tong, L. Zhang, Y. Sakurai, D.R. Myers, L. Hong, W.A. Lam, G. Bao, Nat. Commun. **8**, 15594 (2017). https://doi.org/10.1038/ncomms15594
130. E.Y. Yu, M. Bishop, B. Zheng, R.M. Ferguson, A.P. Khandhar, S.J. Kemp, K.M. Krishnan, P.W. Goodwill, S.M. Conolly, Nano Lett. (2017). https://doi.org/10.1021/acs.nanolett.6b04865
131. G. Song, C. Liang, H. Gong, M. Li, X. Zheng, L. Cheng, K. Yang, X. Jiang, Z. Liu, Adv. Mater. **27**, 6110 (2015). https://doi.org/10.1002/adma.201503006
132. A.P. Khandhar, P. Keselman, S.J. Kemp, R.M. Ferguson, P.W. Goodwill, S.M. Conolly, K.M. Krishnan, Nanoscale **9**, 1299 (2017). https://doi.org/10.1039/c6nr08468k
133. H. Kobayashi, R. Watanabe, P.L. Choyke, Theranostics **4**, 81 (2014). https://doi.org/10.7150/thno.7193
134. C. Martinez-Boubeta, K. Simeonidis, A. Makridis, M. Angelakeris, O. Iglesias, P. Guardia, A. Cabot, L. Yedra, S. Estradé, F. Peiró, Z. Saghi, P.A. Midgley, I. Conde-Leborán, D. Serantes, D. Baldomir, Sci. Rep. **3**, 1652 (2013). https://doi.org/10.1038/srep01652
135. R. Hergt, R. Hiergeist, M. Zeisberger, D. Schüler, U. Heyen, I. Hilger, W.A. Kaiser, J. Magn. Magn. Mater. **293**, 80 (2005). https://doi.org/10.1016/j.jmmm.2005.01.047
136. J.G. Ovejero, D. Cabrera, J. Carrey, T. Valdivielso, G. Salas, F.J. Teran, Phys. Chem. Chem. Phys. **18**, 10954 (2016). https://doi.org/10.1039/c6cp00468g
137. M.E. Sadat, R. Patel, J. Sookoor, S.L. Bud'Ko, R.C. Ewing, J. Zhang, H. Xu, Y. Wang, G.M. Pauletti, D.B. Mast, D. Shi, Mater. Sci. Eng. C **42**, 52 (2014). https://doi.org/10.1016/j.msec.2014.04.064
138. D.F. Coral, P. Mendoza Zélis, M. Marciello, M.D.P. Morales, A. Craievich, F.H. Sánchez, M.B. Fernández Van Raap, Langmuir **32**, 1201 (2016). https://doi.org/10.1021/acs.langmuir.5b03559
139. L.C. Branquinho, M.S. Carrião, A.S. Costa, N. Zufelato, M.H. Sousa, R. Miotto, R. Ivkov, A.F. Bakuzis, Sci. Rep. **3**, 2887 (2013). https://doi.org/10.1038/srep02887
140. E. Rapoport, D. Montana, G.S.D. Beach, Lab Chip **12**, 4433 (2012). https://doi.org/10.1039/c2lc40715a
141. G. Vieira, T. Henighan, A. Chen, A.J. Hauser, F.Y. Yang, J.J. Chalmers, R. Sooryakumar, Phys. Rev. Lett. **103**, 128101 (2009). https://doi.org/10.1103/PhysRevLett.103.128101
142. E. Rapoport, G.S.D. Beach, Sci. Rep. **7**, 10139 (2017). https://doi.org/10.1038/s41598-017-10149-9
143. E. Rapoport, G.S.D. Beach, Phys. Rev. B Condens. Matter Mater. Phys. **87**, 174426 (2013). https://doi.org/10.1103/PhysRevB.87.174426.
144. E. Rapoport, G.S.D. Beach, Appl. Phys. Lett. **100**, 082401 (2012). https://doi.org/10.1063/1.3684972
145. M. Donolato, B.T. Dalslet, M.F. Hansen, Biomicrofluidics **6**, 024110 (2012). https://doi.org/10.1063/1.4704520
146. G. Vieira, A. Chen, T. Henighan, J. Lucy, F.Y. Yang, R. Sooryakumar, Phys. Rev. B **85**, 174440 (2012). https://doi.org/10.1103/PhysRevB.85.174440
147. R.D. McMichael, M.J. Donahue, IEEE Trans. Magn. **33**, 4167 (1997). https://doi.org/10.1109/20.619698

148. W.C. Uhlig, M.J. Donahue, D.T. Pierce, J. Unguris, J. Appl. Phys. **105**, 103902 (2009). https://doi.org/10.1063/1.3125526
149. D.T. Chiu, A.J. DeMello, D. Di Carlo, P.S. Doyle, C. Hansen, R.M. Maceiczyk, R.C.R. Wootton, Chem **2**, 201 (2017). https://doi.org/10.1016/j.chempr.2017.01.009
150. Y.M. Wang, X. Cao, G.H. Liu, R.Y. Hong, Y.M. Chen, X.F. Chen, H.Z. Li, B. Xu, D.G. Wei, J. Magn. Magn. Mater. **323**, 2953 (2011). https://doi.org/10.1016/j.jmmm.2011.05.060
151. R. Qiao, C. Yang, M. Gao, J. Mater. Chem. **19**, 6274 (2009). https://doi.org/10.1039/b902394a
152. R.A. Petros, J.M. Desimone, Nat. Rev. Drug Discov. **9**, 615 (2010). https://doi.org/10.1038/nrd2591
153. K.M. Krishnan, IEEE Trans. Magn. **46**, 2523 (2010). https://doi.org/10.1109/TMAG.2010.2046907
154. T.H. Shin, Y. Choi, S. Kim, J. Cheon, Chem. Soc. Rev. **44**, 4501 (2015). https://doi.org/10.1039/c4cs00345d
155. M.W. Ahmad, W. Xu, S.J. Kim, J.S. Baeck, Y. Chang, J.E. Bae, K.S. Chae, J.A. Park, T.J. Kim, G.H. Lee, Sci. Rep. **5**, 8549 (2015). https://doi.org/10.1038/srep08549
156. R. Anbazhagan, Y.A. Su, H.C. Tsai, R.J. Jeng, A.C.S. Appl, Mater. Interfaces **8**, 1827 (2016). https://doi.org/10.1021/acsami.5b09722
157. Y.K. Peng, C.N.P. Lui, Y.W. Chen, S.W. Chou, P.T. Chou, K.K.L. Yung, S.C. Edman Tsang, Nanotechnology **29**, 015102 (2018). https://doi.org/10.1088/1361-6528/aa96eb
158. M. Yang, L. Gao, K. Liu, C. Luo, Y. Wang, L. Yu, H. Peng, W. Zhang, Talanta **131**, 661 (2015). https://doi.org/10.1016/j.talanta.2014.08.042
159. R.M. Ferguson, K.R. Minard, K.M. Krishnan, J. Magn. Magn. Mater. **321**, 1548 (2009). https://doi.org/10.1016/j.jmmm.2009.02.083
160. Y. Du, P.T. Lai, C.H. Leung, P.W.T. Pong, Int. J. Mol. Sci. **14**, 18682 (2013). https://doi.org/10.3390/ijms140918682
161. R. Dhavalikar, C. Rinaldi, J. Appl. Phys. **115**, 074308 (2014). https://doi.org/10.1063/1.4866680
162. L. Kafrouni, O. Savadogo, Prog. Biomater. **5**, 147 (2016). https://doi.org/10.1007/s40204-016-0054-6
163. M.R. Phadatare, J.V. Meshram, K.V. Gurav, J.H. Kim, S.H. Pawar, J. Phys. D. Appl. Phys. **49**, 095004 (2016). https://doi.org/10.1088/0022-3727/49/9/095004
164. S.H. Moon, S.H. Noh, J.H. Lee, T.H. Shin, Y. Lim, J. Cheon, Nano Lett. **17**, 800 (2017). https://doi.org/10.1021/acs.nanolett.6b04016
165. H. Khurshid, J. Alonso, Z. Nemati, M.H. Phan, P. Mukherjee, M.L. Fdez-Gubieda, J.M. Barandiarán, H. Srikanth, J. Appl. Phys. **117**, 17A337 (2015). https://doi.org/10.1063/1.4919250
166. N.A. Usov, B.Y. Liubimov, J. Appl. Phys. **112**, 023901 (2012). https://doi.org/10.1063/1.4737126
167. S.H. Noh, W. Na, J.T. Jang, J.H. Lee, E.J. Lee, S.H. Moon, Y. Lim, J.S. Shin, J. Cheon, Nano Lett. **12**, 3716 (2012). https://doi.org/10.1021/nl301499u
168. N.A. Usov, M.S. Nesmeyanov, V.P. Tarasov, Sci. Rep. **8**, 1224 (2018). https://doi.org/10.1038/s41598-017-18162-8
169. X.L. Liu, Y. Yang, C.T. Ng, L.Y. Zhao, Y. Zhang, B.H. Bay, H.M. Fan, J. Ding, Adv. Mater. **27**, 1939 (2015). https://doi.org/10.1002/adma.201405036
170. S. Ruta, R. Chantrell, O. Hovorka, Sci. Rep. **5**, 9090 (2015). https://doi.org/10.1038/srep09090
171. D.B. Reeves, J.B. Weaver, Appl. Phys. Lett. **104**, 102403 (2014). https://doi.org/10.1063/1.4867987
172. C. Haase, U. Nowak, Phys. Rev. B **85**, 045435 (2012). https://doi.org/10.1103/PhysRevB.85.045435
173. G.T. Landi, Phys. Rev. B **89**, 014403 (2014). https://doi.org/10.1103/PhysRevB.89.014403
174. R. Fu, Y. Yan, C. Roberts, Z. Liu, Y. Chen, Sci. Rep. **8**, 4704 (2018). https://doi.org/10.1038/s41598-018-23225-5
175. S. Dutz, R. Hergt, Nanotechnology **25**, 452001 (2014). https://doi.org/10.1088/0957-4484/25/45/452001

176. M. Johannsen, U. Gneveckow, L. Eckelt, A. Feussner, N. WaldÖFner, R. Scholz, S. Deger, P. Wust, S.A. Loening, A. Jordan, Int. J. Hyperth. **21**, 637 (2005). https://doi.org/10.1080/02656730500158360
177. M. Johannsen, B. Thiesen, P. Wust, A. Jordan, Int. J. Hyperth. **26**, 790 (2010). https://doi.org/10.3109/02656731003745740
178. M.T. Bryan, K.H. Smith, M.E. Real, M.A. Bashir, P.W. Fry, P. Fischer, M.-Y. Im, T. Schrefl, D.A. Allwood, J.W. Haycock, IEEE Magn. Lett. **1**, 1500104 (2010). https://doi.org/10.1109/LMAG.2010.2046143
179. B. Lim, V. Reddy, X. Hu, K. Kim, M. Jadhav, R. Abedini-Nassab, Y.-W. Noh, Y.T. Lim, B.B. Yellen, C. Kim, Nat. Commun. **5**, 3846 (2014). https://doi.org/10.1038/ncomms4846